Supplementary Information

Surface engineering with microstructured gel network for superwetting membranes

Yuandong Jia,[a,b] Kecheng Guan,[a] Pengfei Zhang,[a,b] Qin Shen,[a,b] Shengyao Wang,[a,b] Yuqing Lin,[a] and Hideto Matsuyama*[a,b]*

[a] Y. Jia, Dr. K.Guan, P. Zhang, Q. Shen, S. Wang, Dr. Y. Lin, Prof. H. Matsuyama
Research Center for Membrane and Film Technology, Kobe University, 1-1 Rokkodaicho, Nada, Kobe 657-8501, Japan

[b] Y. Jia, P. Zhang, Q. Shen, S. Wang, Prof. H. Matsuyama
Department of Chemical Science and Engineering, Kobe University, 1-1 Rokkodaicho, Nada, Kobe 657-8501, Japan

* To whom all correspondence should be addressed.
E-mail: guan@people.kobe-u.ac.jp (Dr. K. Guan); matuyama@kobe-u.ac.jp (Prof. H. Matsuyama).

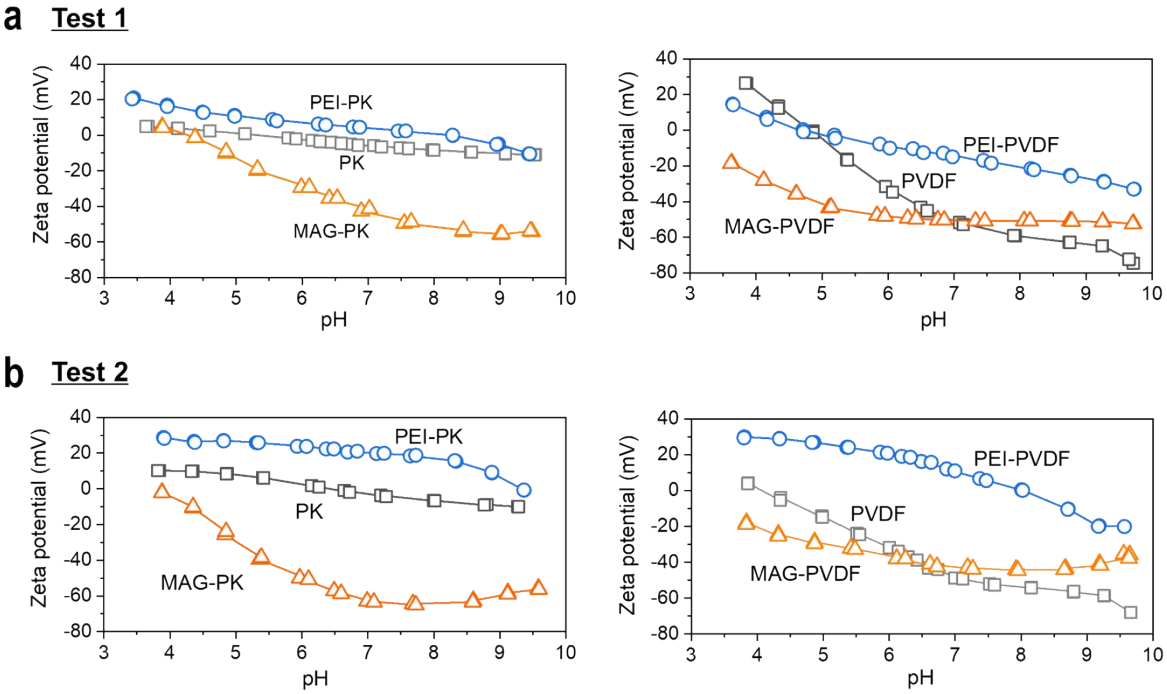

Figure S1. Zeta potential tests of different membrane surfaces: (a) Test 1; (b) Test 2.

Zeta potentials of different membrane surfaces were conducted twice to double-confirm the charge-induced assembly of MAG layer. Taking PK substrate as an example, after PEI being grafted onto the surface, the membrane was revealed as more positively charged among the tested pH range; and then after alginate was introduced, the resulting MAG-PK membrane showed as highly negatively charged. These results confirmed the charge effect between different chemical species on the membrane surface as well as the successful deposition of MAG layer.

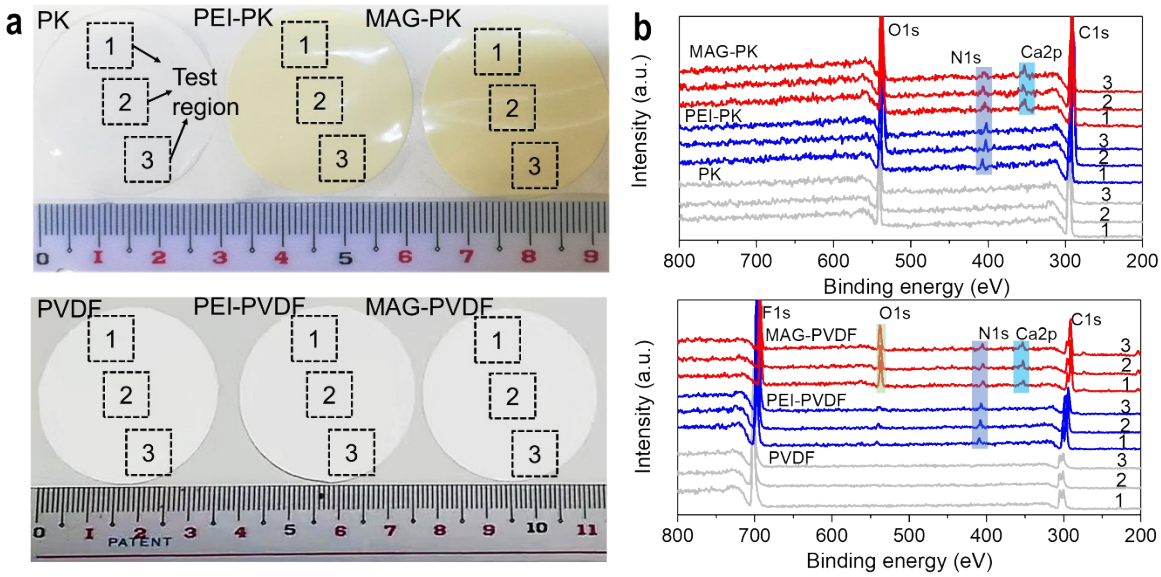

Figure S2. (a) Digital photos showing the selected three test regions from different membranes and (b) Corresponding XPS survey spectra of different membranes in different test regions. The concentrations of PEI and NaAlg aqueous solutions used for modification were 0.5 wt% and 0.4 wt%, respectively.

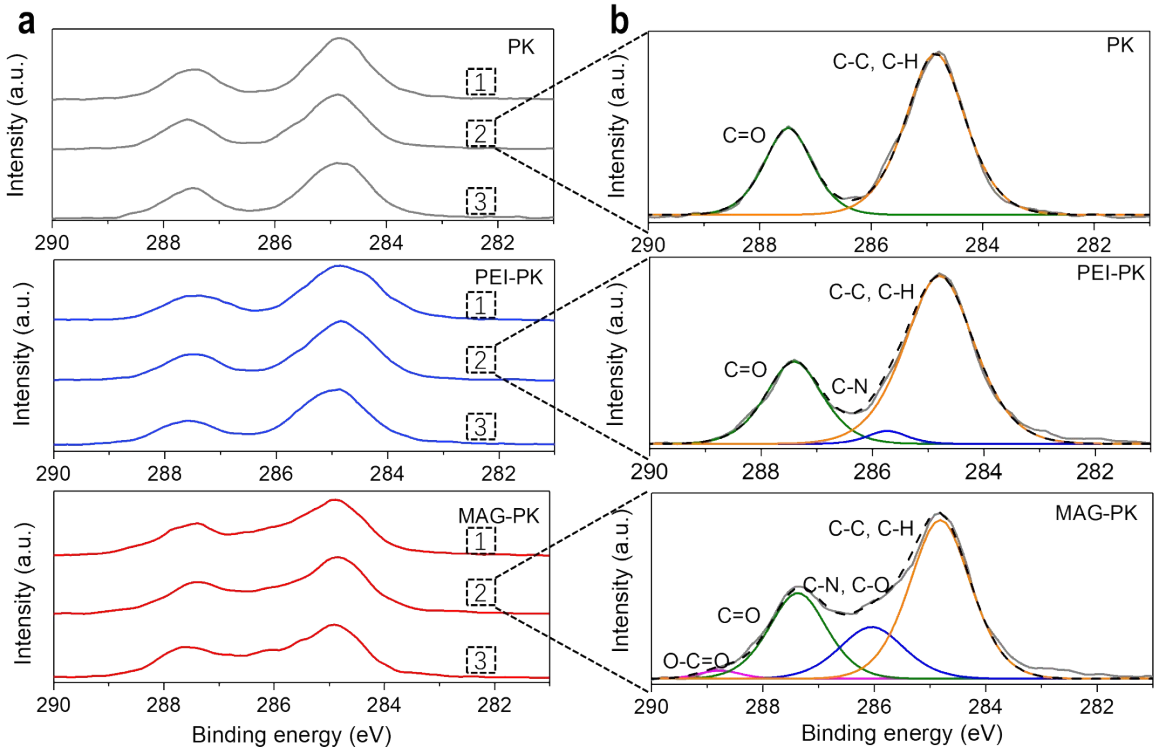

Figure S3. XPS C1s spectra of pristine and modified PK membranes.

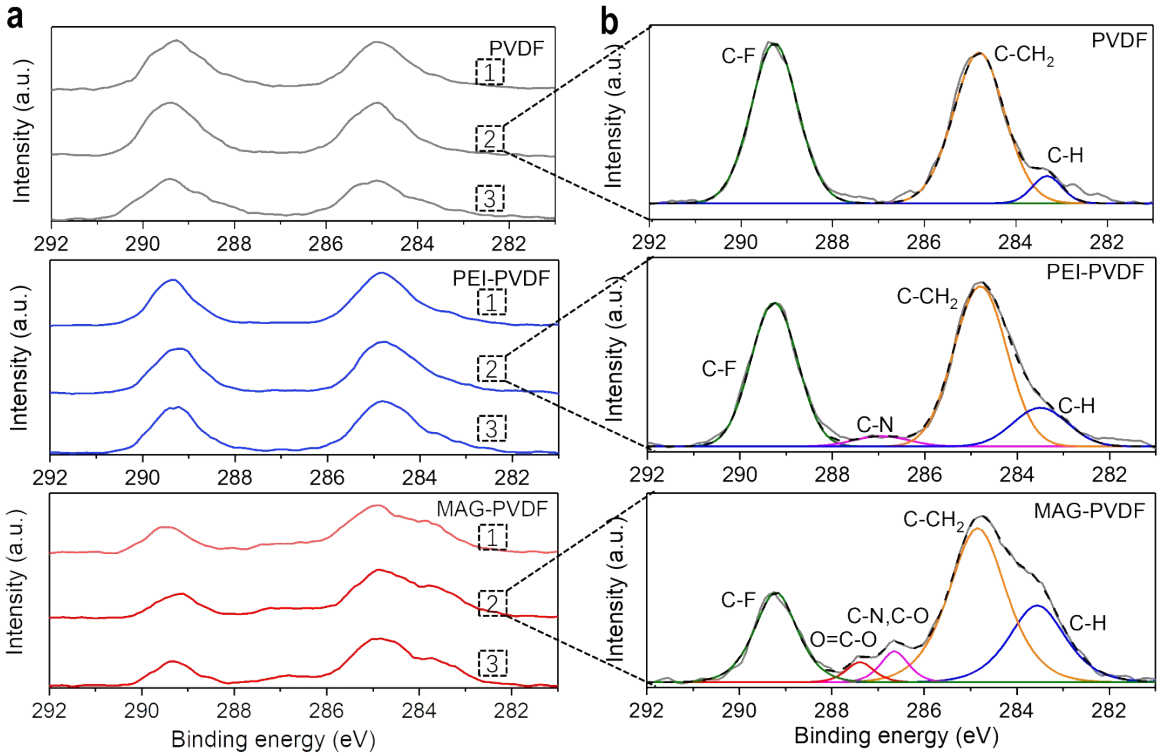

Figure S4. XPS C1s spectra of pristine and modified PVDF membranes.

The XPS spectroscopy was measured to analyze the surface chemistry of the MAG-modified membrane. Different regions of different types of membrane were analyzed by the XPS technique. Similar spectra were obtained for the samples from different regions of each membrane, which indicates that the MAG structure is distributed well on the membrane surface.

The elemental compositions were changed in different membrane samples for PK and PVDF, which was the result of the introduced PEI, NaAlg, and the ionic crosslinker of Ca^{2+}. Taking PK as an example, compared with the C1s spectrum of the original PK membrane, the PEI-PK membrane shows a new peak at a binding energy value of about 285.4 eV, suggesting the –C–N functional group from the PEI. And the MAG-PK displays a distinct peak around 288.2 eV, which is attributed to the carboxyl groups from NaAlg decoration on membrane surface.

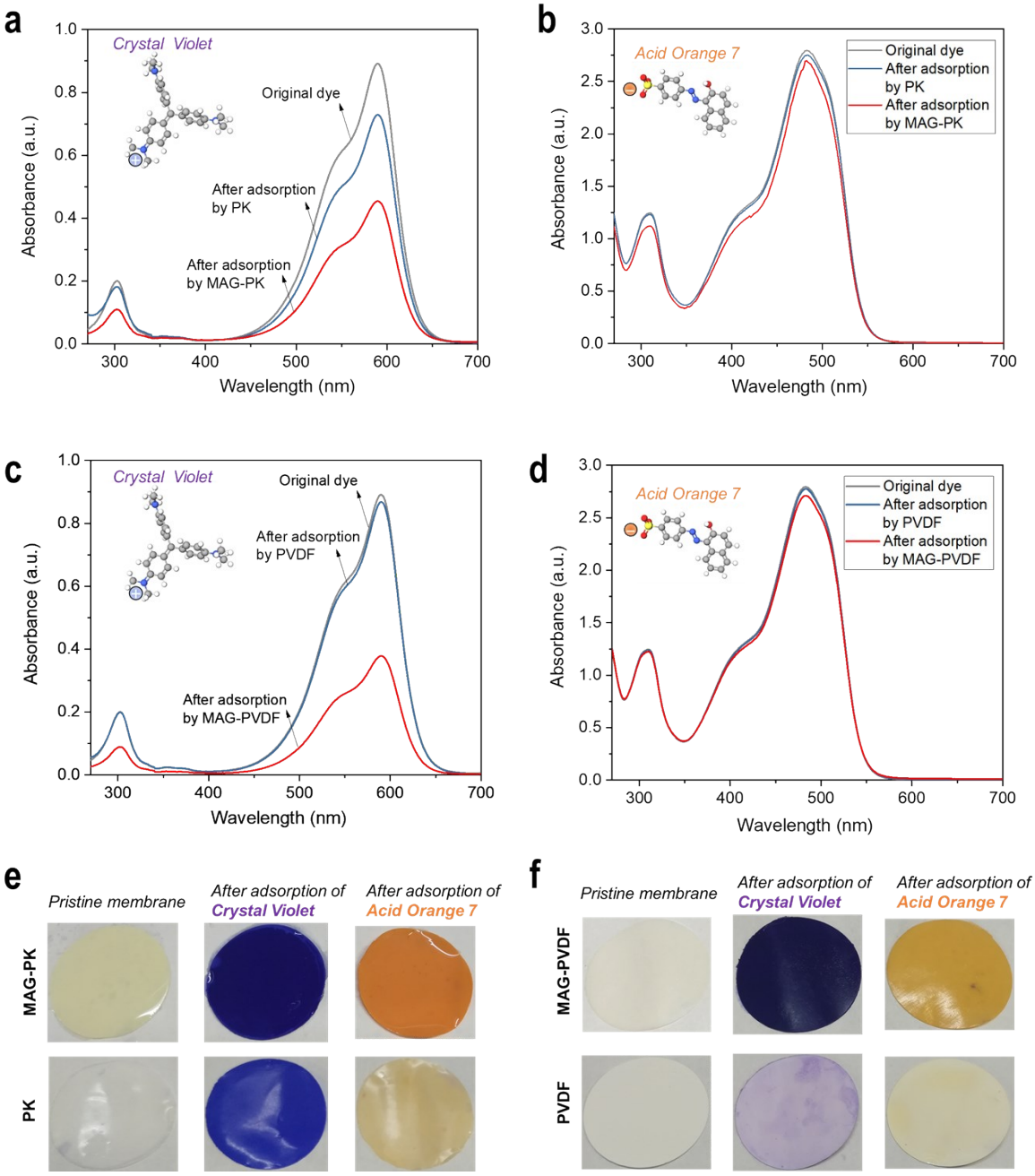

Figure S5. UV-vis spectra of (a,c) Crystal Violet and (b,d) Acid Orange 7 dye solution before and after adsorption by PK, MAG-PK, PVDF, and MAG-PVDF membranes; (e,f) Digital photos of PK, MAG-PK, PVDF, and MAG-PVDF membranes before and after dye adsorption.

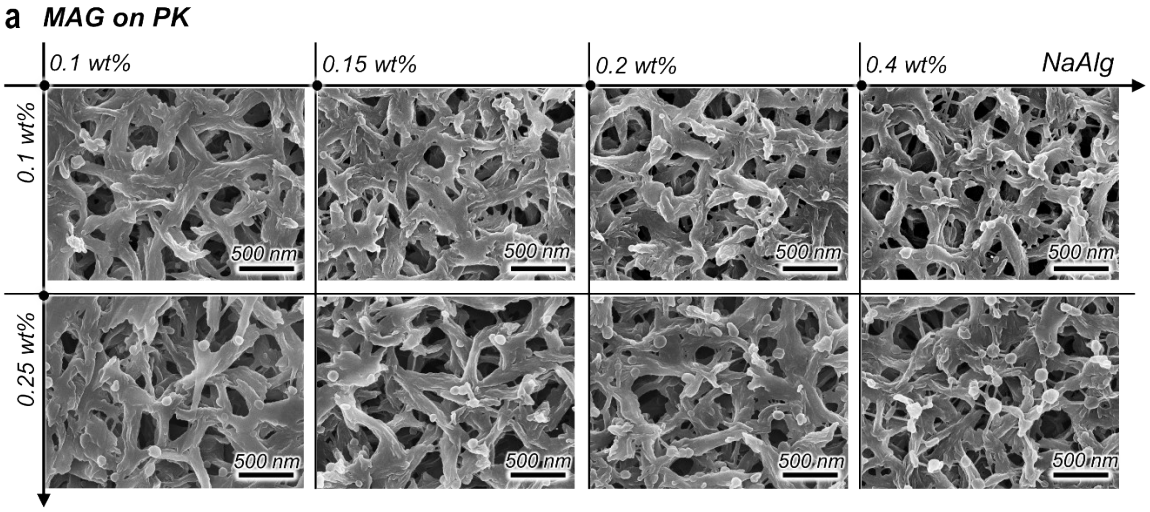

Figure S6. The SEM images of the morphologies of MAG formed on the PK substrates using different concentrations of NaAlg and PEI.

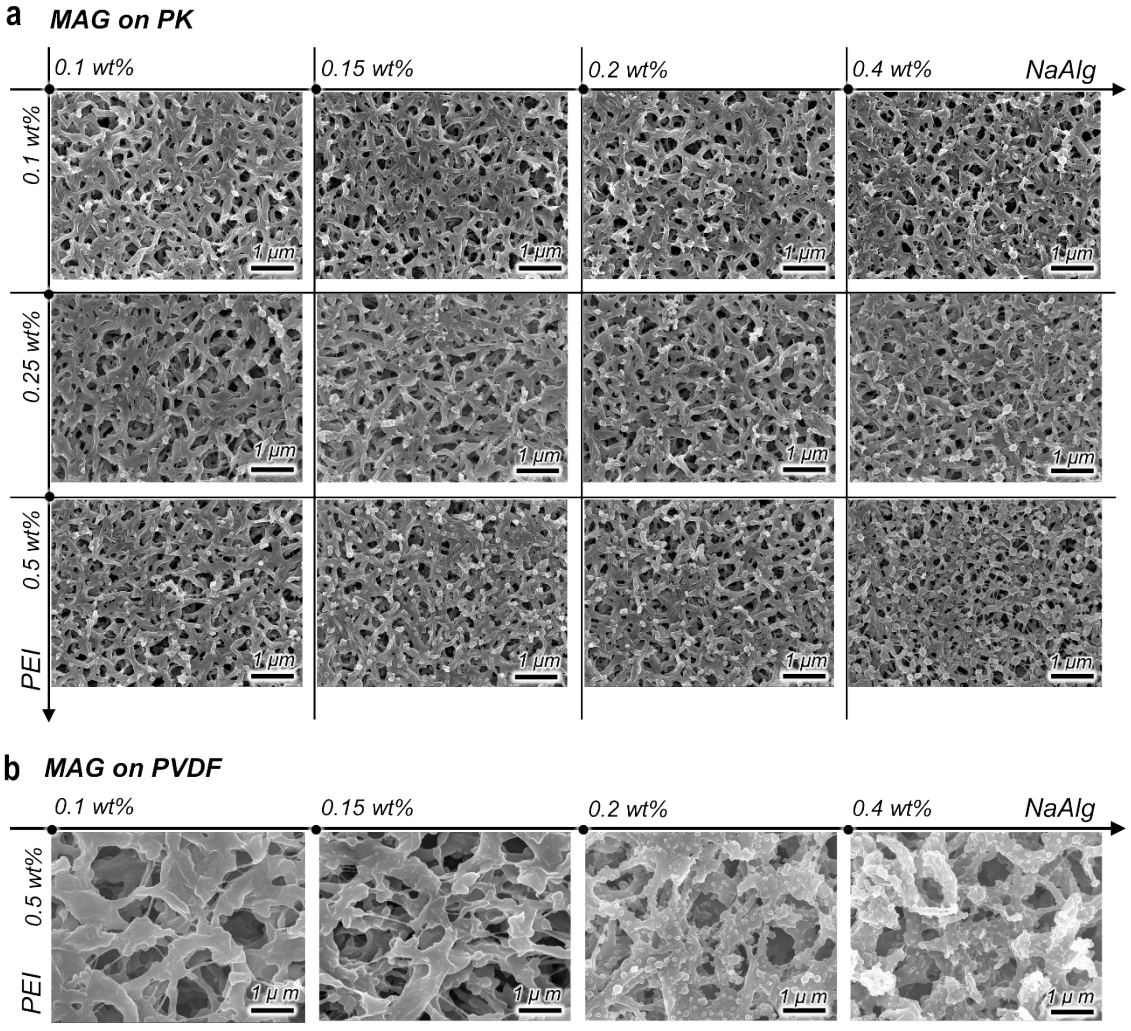

Figure S7. Lower-magnification SEM images of the morphologies of MAG formed on (a) PK and (b) PVDF substrates using different concentrations of NaAlg and PEI.

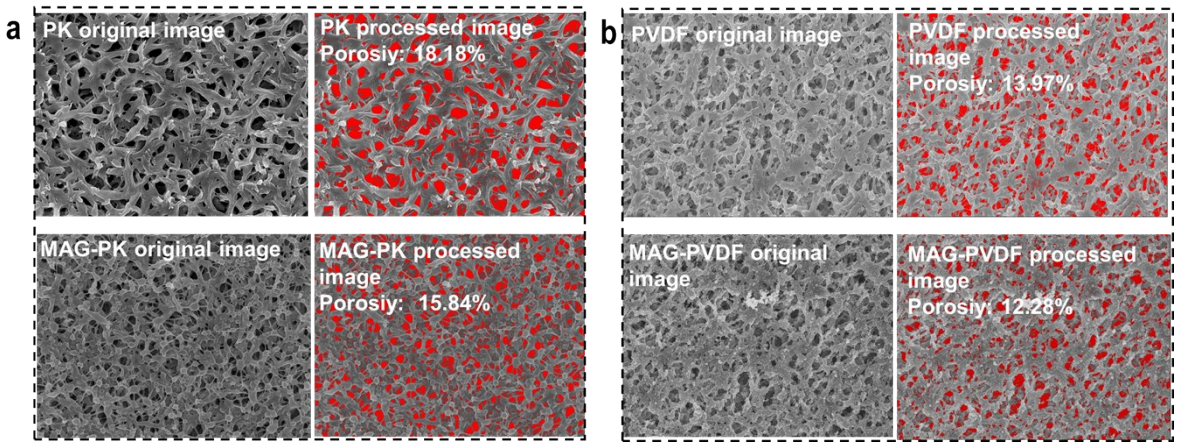

Figure S8. The original and processed SEM images of (a) PK and MAG-PK, (b) PVDF and MAG-PVDF membranes for surface porosity analysis.

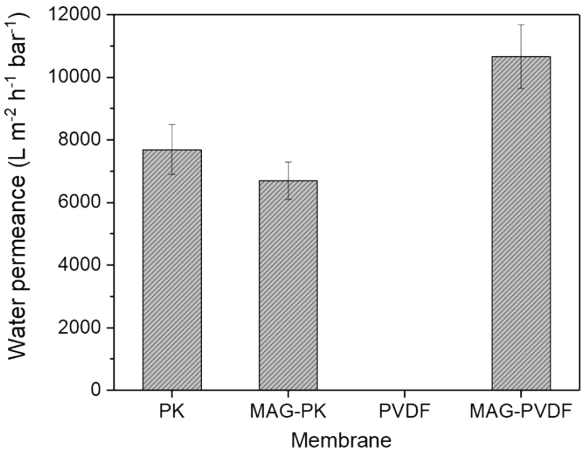

Figure S9. Pure water permeance of the pristine PK, MAG-PK, and MAG-PVDF membranes. The concentrations of PEI and NaAlg aqueous solutions for MAG modification were 0.5 wt% and 0.4 wt%, respectively. The water permeance data was not available for pristine PVDF membrane because of its hydrophobicity not allowing water penetration.

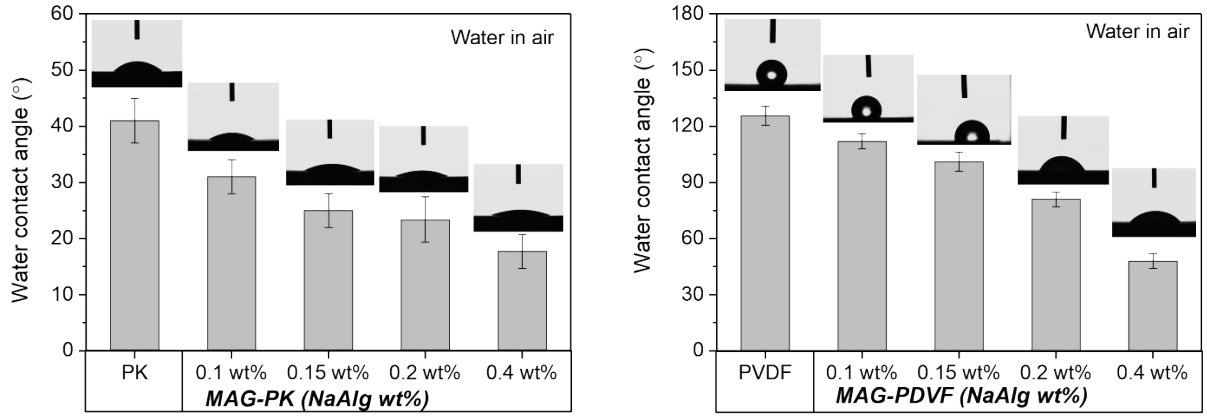

Figure S10. Water contact angle in air for different membranes.

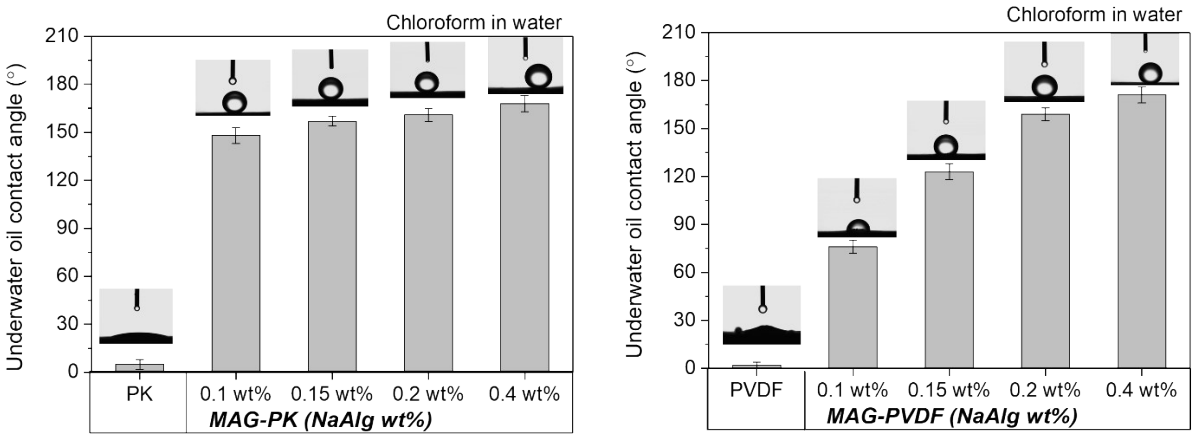

Figure S11. Underwater chloroform oil contact angle for different membranes.

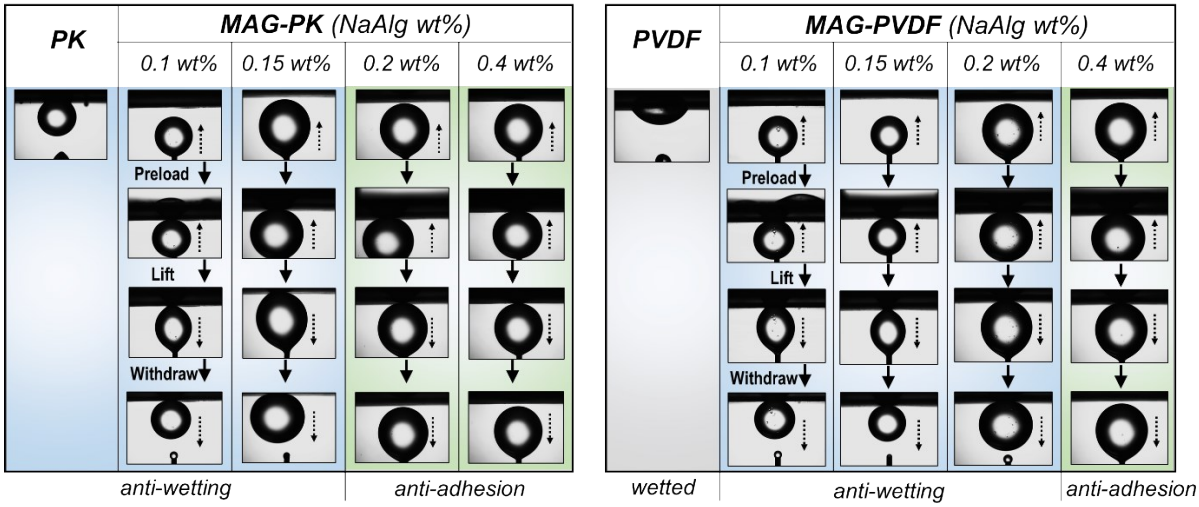

Figure S12. Dynamic underwater soybean oil contact angles for different membranes.

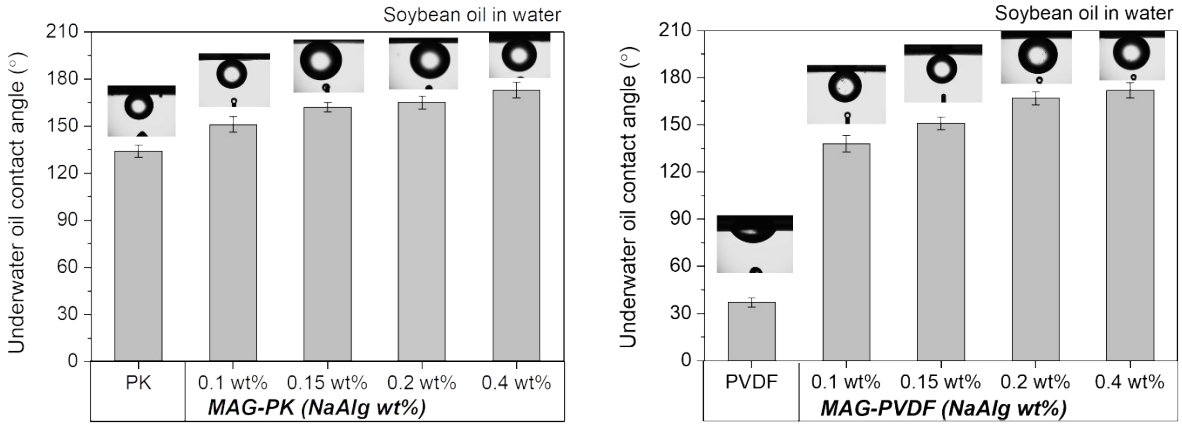

Figure S13. Underwater soybean oil contact angles for different membranes.

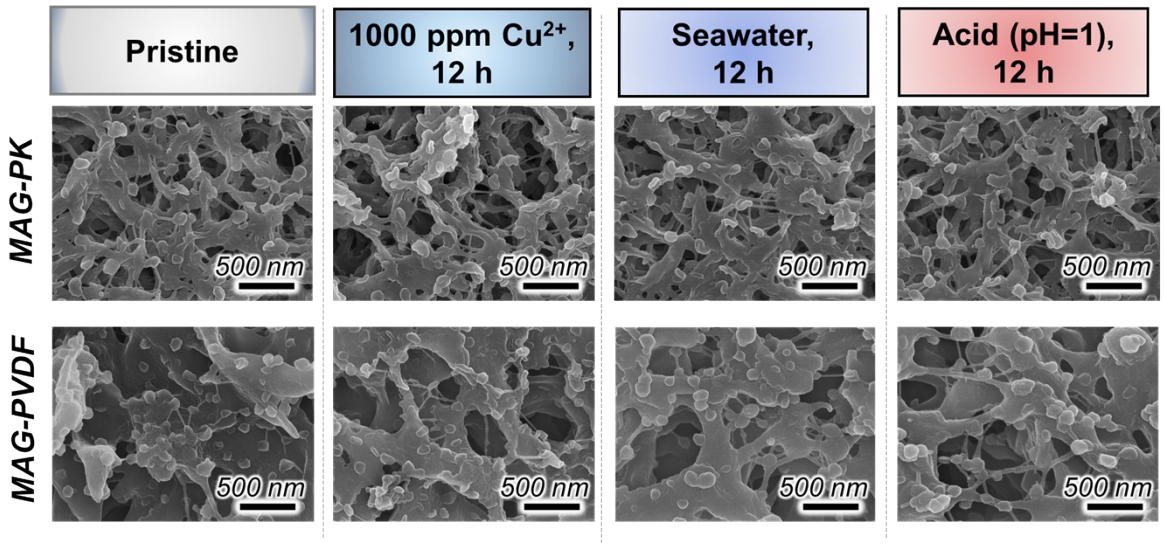

Figure S14. SEM images of MAG-PK and MAG-PVDF membranes before and after exposure to different chemical environments for 12 h each.

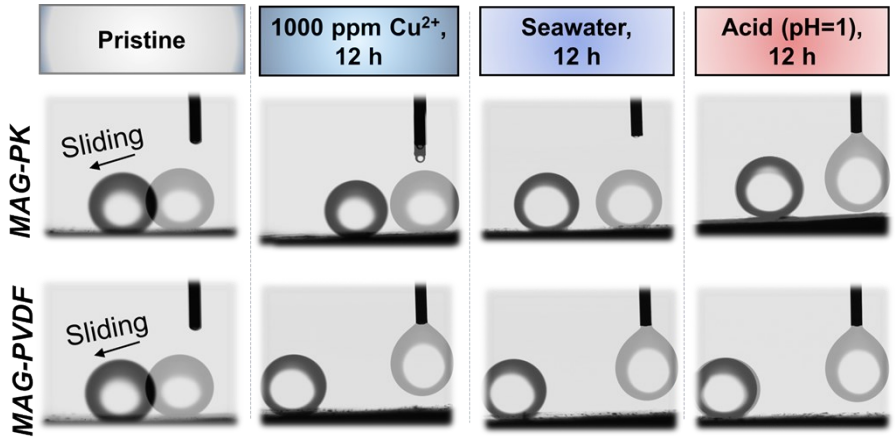

Figure S15. Underwater chloroform oil sliding angles of MAG-PK and MAG-PVDF membranes before and after exposure to different chemical environments for 12 h each.

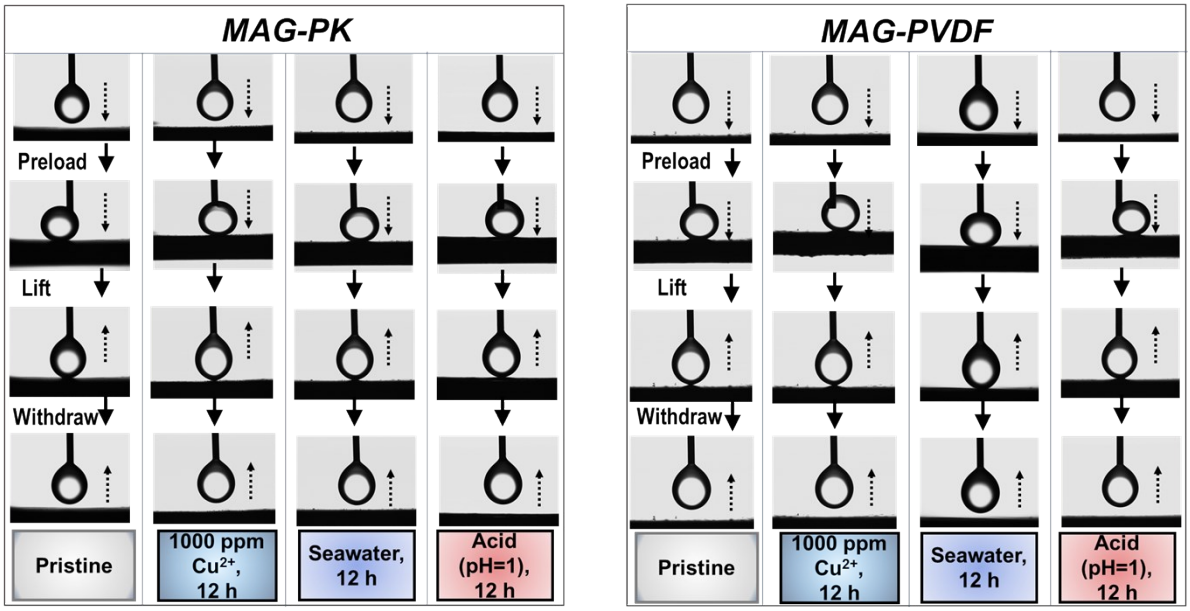

Figure S16. Dynamic oil-adhesion tests of MAG-PK and MAG-PVDF membranes before and after exposure to different chemical environments for 12 h each.

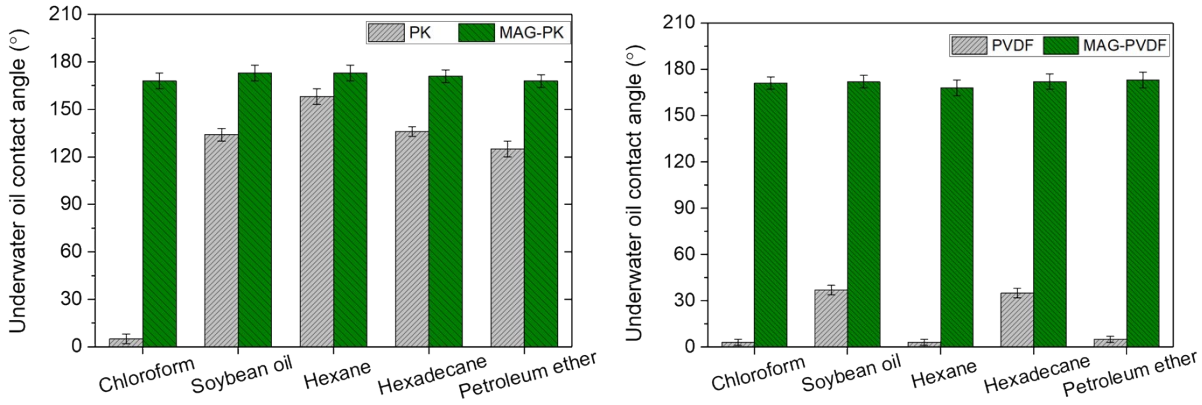

Figure S17. Underwater oil contact angles of PK, MAG-PK, PVDF, and MAG-PVDF membranes.

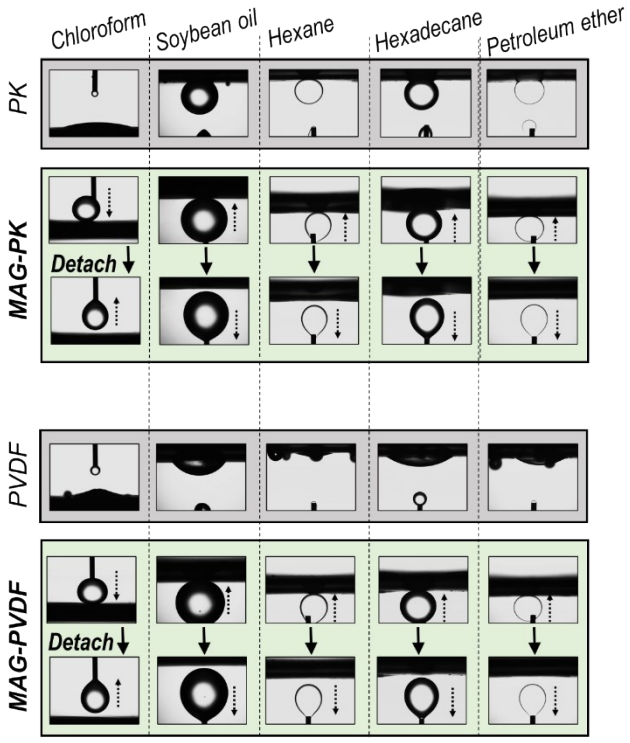

Figure S18. Underwater oil adhesion tests of PK, PVDF, MAG-PK, and MAG-PVDF membranes for different oils.

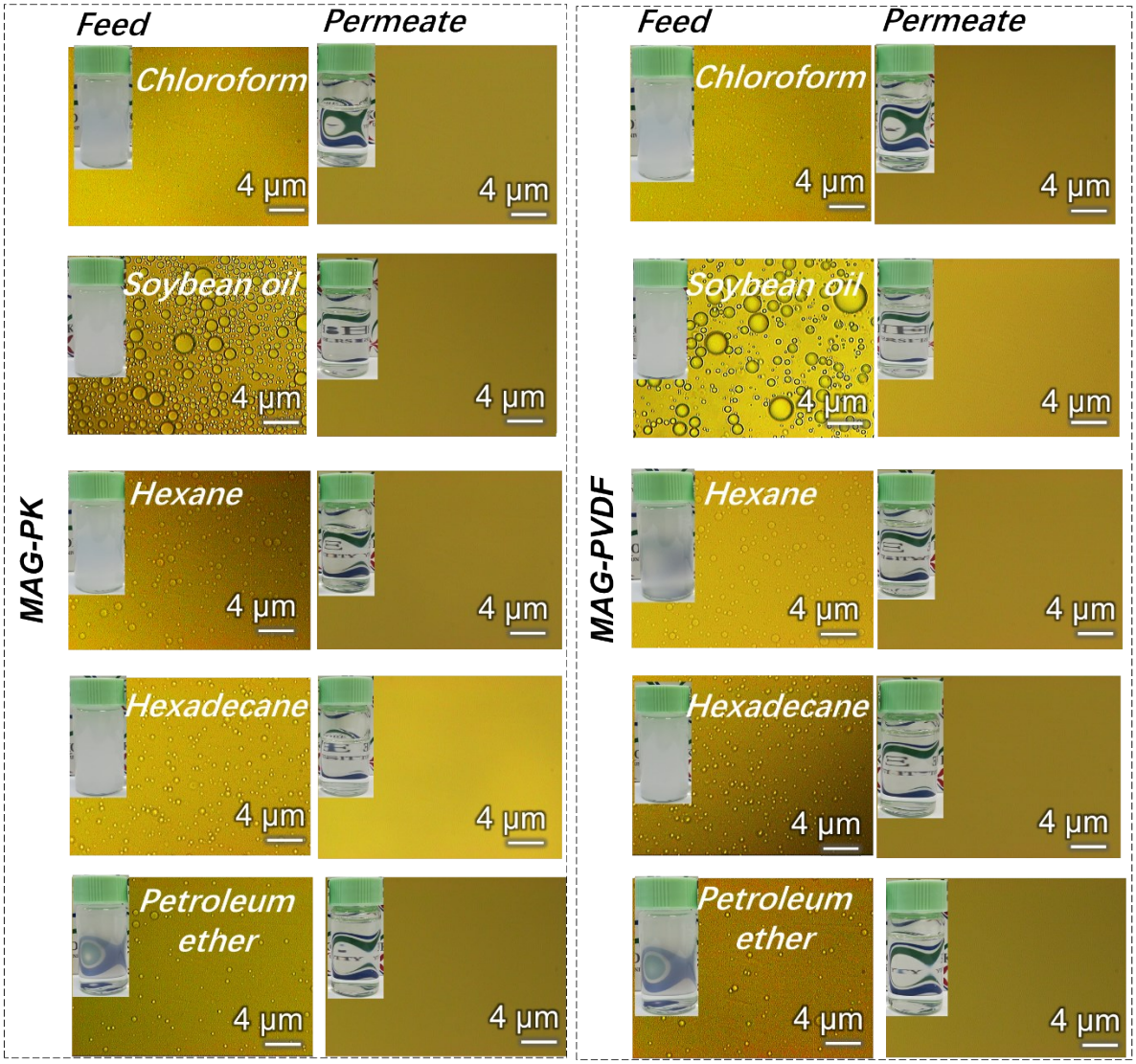

Figure S19. Optical microscope images of the different oil O/W emulsions before/after membrane filtration.

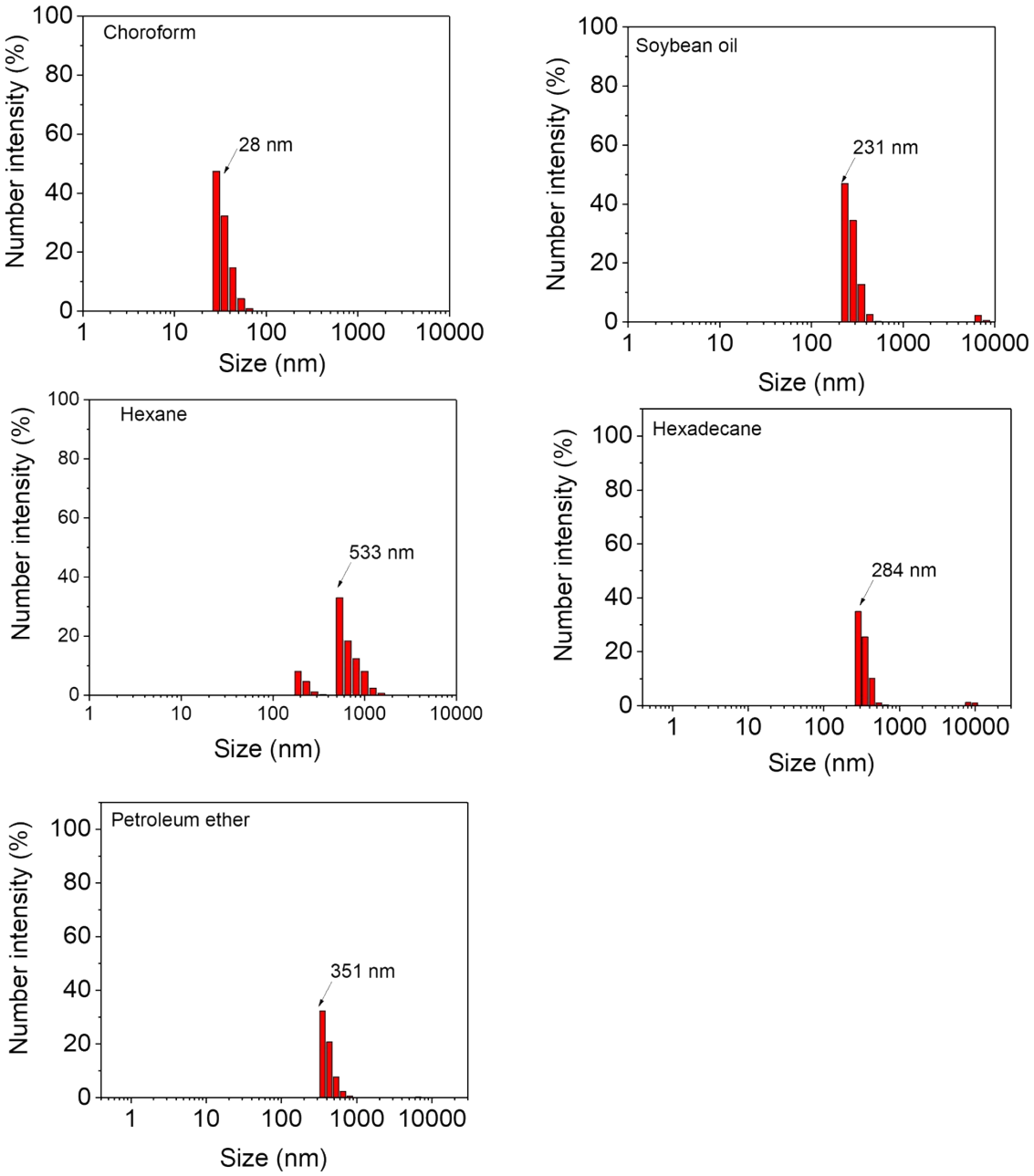

Figure S20. Oil droplet size distributions of different oil O/W emulsions.

The oil droplet size in chloroform O/W emulsion is relatively smaller than other types of emulsions.

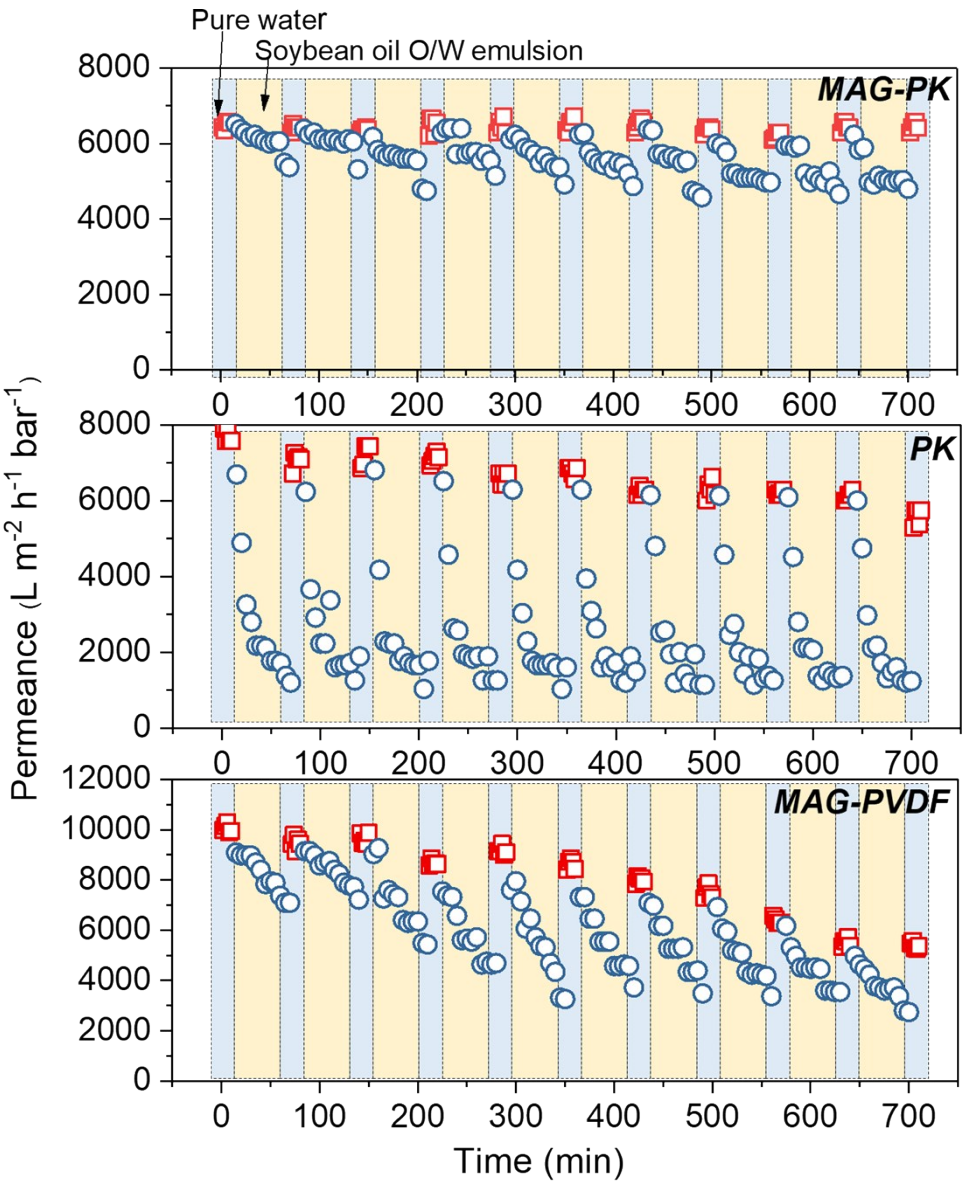

Figure S21. Repeated cycles of the soybean oil O/W emulsion filtration by different membranes.